Reflectance characterization of tape-based plasma mirrors

B. H. Shaw, S. Steinke, J. van Tilborg, and W. P. Leemans

Citation: Physics of Plasmas **23**, 063118 (2016); doi: 10.1063/1.4954242
View online: http://dx.doi.org/10.1063/1.4954242
View Table of Contents: http://scitation.aip.org/content/aip/journal/pop/23/6?ver=pdfcov
Published by the AIP Publishing

Reflectance characterization of tape-based plasma mirrors

B. H. Shaw,[1,2] S. Steinke,[1] J. van Tilborg,[1] and W. P. Leemans[1,a)]
[1]Lawrence Berkeley National Laboratory, Berkeley, California 94720, USA
[2]Applied Science and Technology, University of California, Berkeley, California 94720, USA

(Received 8 March 2016; accepted 7 June 2016; published online 28 June 2016)

Specular reflections of relativistic laser pulses from an overdense plasma mirror (PM) were studied experimentally. The pointing stability of the PM and reflectance of the input laser were characterized. The solid material used for the PM was a VHS tape. This study was done for the magnetic and plastic sides of the VHS tape, and for input light of both s and p-polarizations. The laser pulse fluence was varied by changing the focus position relative to the tape surface, which changed the spot size at the tape. The pointing fluctuations of the reflected pulses caused by the PM were $\simeq 1$ mrad. A peak reflectance of 82% was obtained from the plastic surface of the VHS tape when focusing s-polarized light 4 mm from the tape surface (the wavefront quality was confirmed to be conserved). An analytic model was developed to understand the physics of the interaction for each tape material and polarization. Fitting of our model parameters to the experimental results allowed an estimate of the key plasma parameters such as plasma expansion velocity, ionization intensity, and fraction of absorbed laser energy. *Published by AIP Publishing.*
[http://dx.doi.org/10.1063/1.4954242]

I. INTRODUCTION

When an intense laser pulse interacts with a solid surface, ionization of the solid occurs creating a surface plasma. If ionization occurs close to the temporal peak of the laser pulse, the plasma can remain at high enough density with a flat critical surface to spectrally reflect the pulse. As the surface plasma expands, the critical surface can develop convex-like structure and the percentage of the laser pulse which is specularly reflected decreases. One challenge of using the plasma mirror (PM) experimentally is that the formation of a surface plasma is destructive to the solid target, and hence after each shot an undamaged surface must be provided. This paper explores the use of a thin, spooled tape surface as a PM, which allows for tens of thousands of shots on target.[1,2]

PMs are conventionally used to provide contrast enhancement[3–7] of laser pulses. With a high quality reflection and minimal pointing fluctuations, a PM can also be used as a steering optic near focus where damage to a conventional mirror would occur.

A tape drive has been developed and optimized at the BELLA Center at the Lawrence Berkeley National Laboratory, which spools 1/2 in. wide VHS tapes of 15 μm of thickness.[8] Pointing fluctuations of $\simeq 1$ mrad and reflectance of 82% make this a novel, replaceable, steering mirror which can be positioned near the focus of an intense laser pulse. This PM has found recent applications in active plasma lens[9] and staged acceleration[10] experiments.

II. TAPE DRIVE

A. Chemical structure and material make up of magnetic recording tapes

The VHS tape used in this study is composed of a plastic base which supports a mixture of a polymer bonder and magnetic Iron oxide particles on the front surface.[8] The volume ratio of polymer binder to the iron oxide is $\sim 9/1$, and a mass ratio of the materials is $\sim 1/1$. The VHS tape used in this study is 15 μm thick (13.5 μm thick plastic substrate with 1.5 μm thick bonder/iron layer).[8]

B. Experimental layout

The plasma mirror characterization was performed in the setup sketched in Fig. 1. A laser pulse of 650 mJ with a duration of 40 fs was focused using an f/25 off-axis parabolic mirror (OAP) to a spot size of $w_0 = 22$ μm. The laser fluence on the tape was varied by changing the spot size of the laser at the tape. The focal position was scanned along the propagation axis by translating the OAP and final turning mirror together, which maintains the transverse position of the spot.

Before entering the all-reflective imaging telescope, which is shown and fully described in Ref. 11, the laser pulses were attenuated by a reflection of an optically flat glass wedge at an incident angle of 45° ($\sim$1% reflection), placed 1.28 m downstream of the high-powered laser focus. The telescope itself consisted of a pair of concave and convex mirrors. A fold mirror in between the two curved optics, ensured aberration-free imaging of the focal plane of the laser. The concave mirror was 152.4 mm in diameter with a radius of curvature $R_c = 1200$ mm. The convex mirror was 101.6 mm in diameter with $R_c = 820$ mm. The concave mirror was placed 2 m from the target, and the convex mirror was placed 0.5 m further downstream. The concave mirror determined the angular acceptance of f/13. This telescope provided a transverse magnification of 3.3.

The tape drive consisted of two motorized rotating spools holding the tape, polished metallic rods which the tape was woven around to position the tape at 45° with respect to the input beamline, and a linear encoder used to track the movement of the tape. Prior to a shot being

a)Electronic mail: WPLeemans@lbl.gov

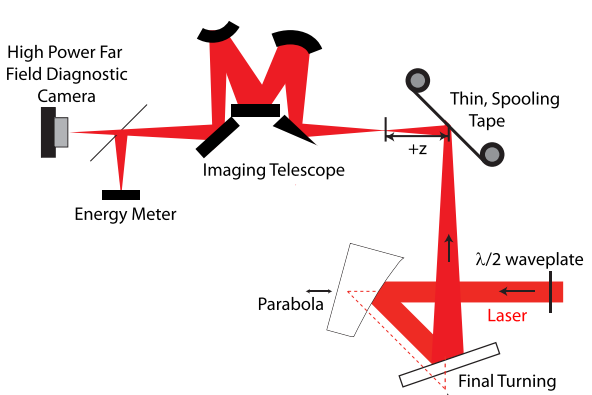

FIG. 1. A schematic of the setup used to characterize the tape-based PM is shown. Characterization of the PM includes measuring the percent of laser energy reflected by the PM and pointing stability of the reflected pulses. The focus is placed a distance z from the tape surface, where $z > 0$ represent downstream of the tape surface. The pointing fluctuations were measured by the high power far field diagnostic.

fired, the tape was held stationary by counter-rotating the two spools with equal force.

The optical image of the laser mode at the target was recorded using a 12-bit CCD camera, referred to as a high power far field diagnostic. By placing the high power far field diagnostic after the reflective telescope, the image plane was able to image a range of ∼15 cm around the beam's focus. Neutral density filters inside a remote-controlled filter wheel were used to attenuate the beam onto the high power far field diagnostic.

An energy meter was used to measure the energy of the reflected laser. This energy meter was calibrated against an upstream energy meter to calculate the reflectance of the PM.

C. Tape monitor diagnostic

The flatness of the tape affects the wavefront quality of the reflected beam. If the tape is held with improper tension, the tape surface tends to bow, ripple, or sag causing the reflected beam to stray from the desired beampath. Therefore, an interlocking feature was employed to ensure the tape surface was flat and correctly angled prior to a laser shot.

The flatness of the tape surface was monitored by a CW, low energy, Helium-Neon (HeNe) laser, reflected off the tape. A cross-hair was used in the HeNe beam as a mask to produce four equally sized and space beamlets. A camera monitored the position of the four beamlets following the tape reflection. If the distance between the beamlets was uniform (as seen in Fig. 2) then the tape was considered to be flat and free of ripples or bowing, and this allowed the system to fire a high-powered shot on target. If unequally spaced beamlets from the HeNe laser's tape reflection were detected by the camera, the software system inhibited a shot from being taken and the tape was spooled again.

D. Pointing fluctuation measurement

A pointing fluctuation measurement of a second low-power, non-ionizing HeNe laser was taken from the reflection

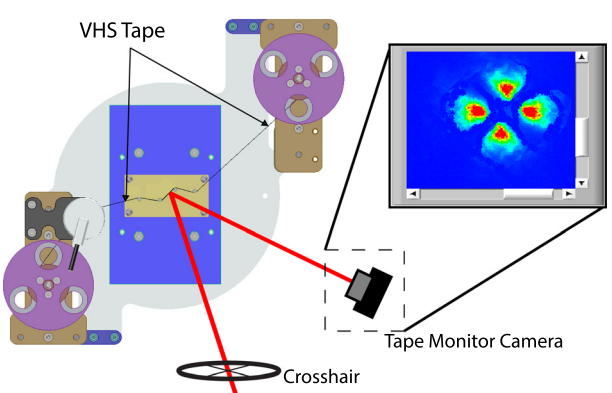

FIG. 2. A schematic of the tape monitor setup consisting of a HeNe laser, cross-hair, reflective tape surface, and camera is shown.

from the tape surface. By not creating a surface plasma, the pointing errors caused by fluctuations of the tape's positioning were measured. The setup included an input HeNe laser, the tape drive spooled with VHS tape, and a CCD camera to measure the position of the reflected laser. The tape was spooled between each acquisition of the CCD camera, and the pointing fluctuation was calculated by means of standard deviation of the beam's centroid.

The fluctuation of the HeNe beam reflected off the non-ionized VHS tape was 310 μrad. The laser jitter of the HeNe laser itself without tape reflection was below the detection accuracy of 40 μrads/pixel.

The pointing fluctuation measurement from the high-power laser reflected off the PM was performed using the setup shown in Fig. 1.

The results of the reflected high-power laser pulse from the PM and input laser jitter at focus are shown in Fig. 3. The

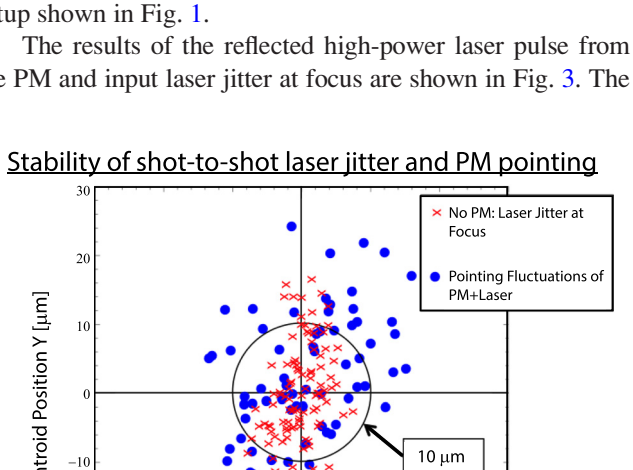

FIG. 3. Results of the pointing study comparing high-power laser jitter at focus and ionized PM reflections. Input laser jitter at focus (red x) and PM pointing fluctuations (blue circles) were measured as the standard deviation of the laser spot's centroid to the beam axis. Pointing fluctuations of the laser at focus were measured as $\Delta x_L = 4.1\ \mu$m and $\Delta y_L = 10\ \mu$m. The imaging telescope was set such that the far field diagnostic was imaging the plane 10 mm downstream of the tape. The PM reflected laser pointing fluctuations were measured as $\Delta x_{PM+L} = 10.3\ \mu$m and $\Delta y_{PM+L} = 14.2\ \mu$m.

reflected pulses off the PM were measured using the far field diagnostic imaging the plane 10 mm downstream of the tape. The focus of the laser was placed 4 mm downstream of the tape. The intensity at the tape remained constant and no other parameters were changed. The PM pointing fluctuations were measured as $\Delta x_{PM+L} = 10.3\ \mu$m and $\Delta y_{PM+L} = 14.2\ \mu$m.

The input laser's pointing fluctuations without a PM were measured at focus as $\Delta x_L = 4.1\ \mu$m and $\Delta y_L = 10\ \mu$m (rms). These fluctuation values are intrinsically included in the value of the pointing fluctuation measured from the reflected PM pulses.

We calculate the pointing fluctuations cause only by the plasma mirror as $\Delta x_{PM}^2 = \Delta x_{PM+L}^2 - \Delta x_L^2$. The results for Δx_{PM} and Δy_{PM} were $\Delta x_{PM} = 9.4\ \mu$m and $\Delta y_{PM} = 10.1\ \mu$m. These values were converted to angular pointing fluctuations of the PM as $\theta_{PM} = 0.94$ mrad in x and $\theta_{PM} = 1.0$ mrad in y.

III. PLASMA MIRROR

A. Reflectance results

The experiment of the reflectance of s-polarized light and p-polarized light was studied using the iron oxide surface and plastic surface of a VHS tape as the plasma mirror.

The results of the study are given in Fig. 4. By changing the focal location with respect to the position of the tape, the peak intensity of the pulse on the tape was changed.

The maximum reflectance of 82% was obtained when the focus was 4 mm (~2 Rayleigh lengths) from the VHS plastic surface. The maximum reflectance of the VHS iron oxide surface was produced when the focus was 14 mm from the tape surface.

The amount of reflectance decreased when changing the input light from s to p-polarization using a $\lambda/2$ waveplate. The lower reflectance values for the p-polarization measurements were caused by Brunel[12] and resonance absorption[13] of p-polarized light, which provided a measurement of their combined effects (see discussion in Sec. IV E).

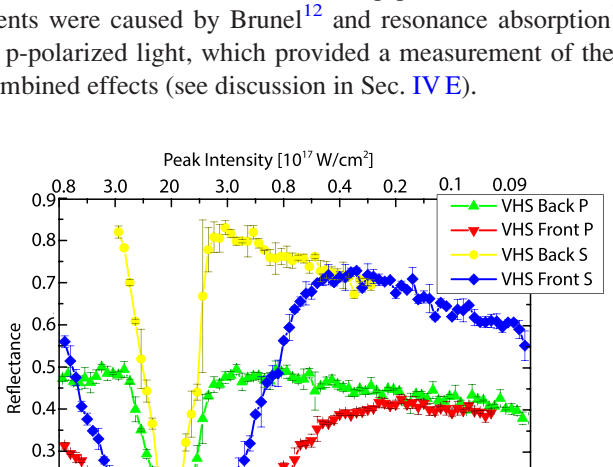

FIG. 4. Plot showing the reflected energy from both the plastic (Back) and iron oxide (Front) sides of a VHS tape plasma mirror using s and p-polarized light. The focal position of the laser pulse was scanned longitudinally in order to scan the input intensity of the laser pulse at the tape surface.

B. Wavefront quality conservation

Figure 5 shows a direct comparison of the focal mode quality of the vacuum and PM reflected pulses at focus and one Rayleigh length upstream and downstream of focus. The measurement was performed by translating the location the optics of the imaging telescope shown in Fig. 1. For the case of the PM reflected data, the position of the focus was placed +4 mm from the plastic surface of the VHS tape, which produced the peak reflectance of 82% and had an intensity of 4×10^{17} W/cm^2 at the tape surface.

The plots [Figs. 5(a) and 5(c)] of the beam radius, ω, show the vacuum and PM reflected laser modes through focus in x and y. The overlap between the plots for spot size x and spot size y are seen when astigmatism in the beam is minimized and the mode is Gaussian through focus.

The laser modes are shown at −2 mm from focus, at the focal plane, and +2 mm from focus for both the vacuum and PM reflected laser modes. By comparing the mode quality of vacuum focal modes to the PM reflected modes, the shape and focusability of the PM modes match the high quality focus seen in the vacuum focal scan. This conservation of wavefront quality near focus confirms that the quality of the laser pulse's wavefront is conserved during the PM reflection.

IV. PLASMA MIRROR MODEL

A heuristic numerical model was developed to calculate the amount of light reflected from the PM surface and accounts for the laser energy absorbed by the plasma, the shape (or surface roughness) of the PM at the peak of the laser pulse, and the intensity distribution of the spot size on the tape.

We calculate the reflectance as

$$R(z) = (1 - \alpha) r(z) S(z), \tag{1}$$

where α is the percentage of input light absorbed by the surface plasma, r(z) is the percentage of light specularly reflected from a surface with a given roughness, and S(z) is a spatial term that calculates the area ratio of the laser spot where ionization occurred prior to the temporal peak of the pulse.

A. Laser pulse's temporal shape and focal characteristics

The contrast ratios of the picosecond shoulder and amplified spontaneous emission (ASE) pedestal were measured by a high dynamic range third-order cross-correlator (SEQUOIA from Amplitude Technologies). The temporal intensity of the main peak was measured by a GRENOUILLE[14] (Swap Optics). The 40 fs FWHM main peak, the picosecond shoulder from −5 to +5 ps, and the amplified spontaneous emission (ASE) pedestal which reaches out beyond nanoseconds are shown in Fig. 6.

To describe the laser pulse, three Gaussian functions were added together which represent main peak, the picosecond shoulder, and the ASE pedestal. The temporal profile of the laser pulse was measured as

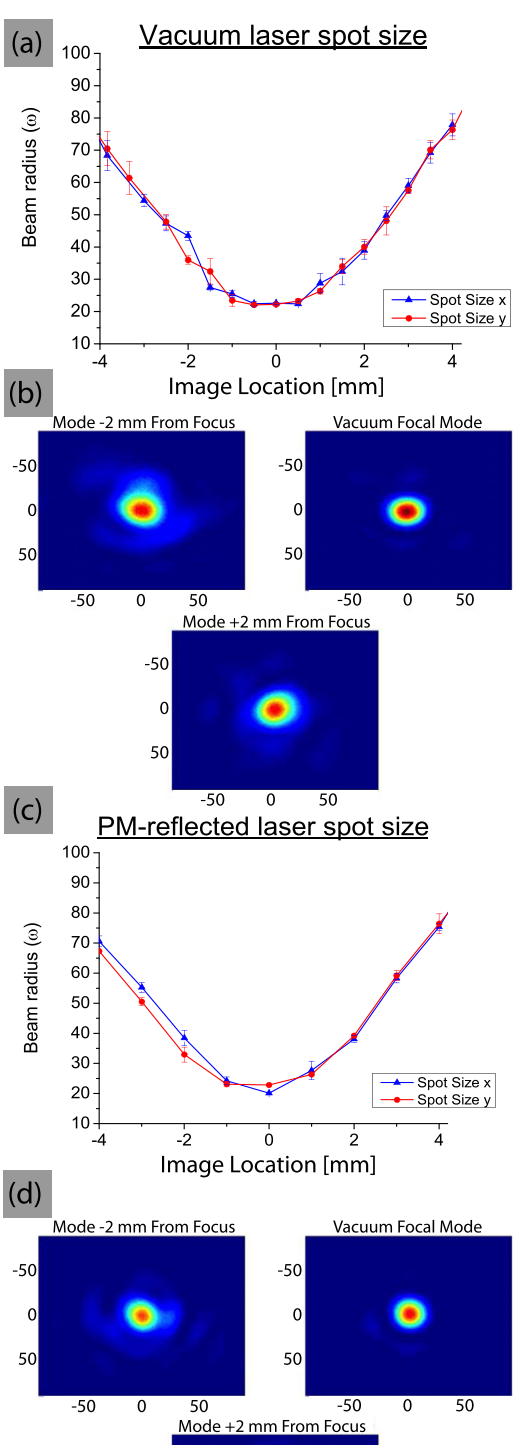

FIG. 5. The plot of the FWHM in x and y for the vacuum laser focal mode [Plot (a)] and the PM reflected laser focal mode [Plot (c)] through focus. The laser modes are shown at −2 mm from focus, at the focal plane, and +2 mm from focus for the vacuum focus [Images (b)] and from the PM reflection [Images (d)]. The mode quality of the images is compared to the focal images of the PM reflected modes. The laser mode from the PM reflection is high quality and matches the focal mode quality of the vacuum focus, which implies a conservation of the wavefront quality. The PM reflected modes were obtained at an incident PM intensity of 4×10^{17} W/cm^2.

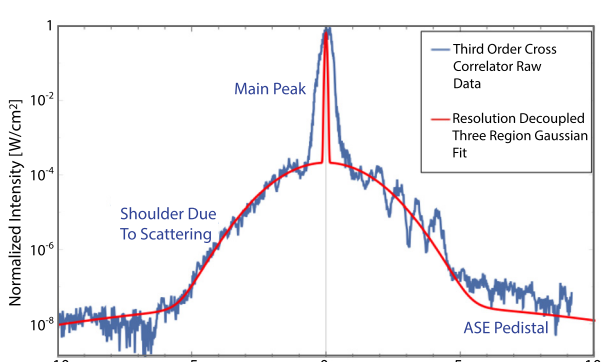

FIG. 6. Normalized third-order cross-correlation measurement used to characterize the temporal shape of the pulse's intensity. The three regions of the cross-correlation (blue) are shown and labeled. The width of the main peak in our resolution-decoupled fit was 40 fs FWHM measured by a GRENOUILLE. At focus the peak intensity of the pulse was 2×10^{18} W/cm^2.

$$I[t] = I_{Tape} \times \sum_{i=1}^{3} A_i e^{\frac{-(t-\mu_i)^2}{2\sigma_i^2}}. \tag{2}$$

The coefficients for A, μ, and σ of each of the three regions are given in Table I. I_{Tape} is given by

$$I_{Tape} = \frac{2E}{\pi w(z)^2 \tau}, \tag{3}$$

where E is the energy of the pulse in Joules, $\pi w(z)^2$ gives the area of the beam on the tape, and τ is the pulse duration. For the peak of the pulse, we use the duration (measured by a GRENOUILLE) of $\tau = 40$ fs (FWHM). The energy in the laser beam onto the tape was 650 mJ. These pulse characteristics yielded a maximum peak intensity on tape of 2×10^{18} W/cm^2.

The size of the beam through focus was used to determine the intensity of the beam when it interacts with the tape. The beam waist was measured to be $w_0 = 22\,\mu$m. The dependence of the beam radius through focus is modeled by Gaussian beam propagation as

$$w(z) = w_0 \times \sqrt{1 + \left(\frac{z}{z_R}\right)^2}, \tag{4}$$

with $z_R = \pi w_0^2/\lambda$, and $\lambda = 800$ nm.

B. Determination of the plasma parameters

The key plasma parameters from our model, such as ionization intensity, plasma expansion velocity, and absorption, could be obtained by fitting them to the experimental laser reflectance data as a function of focal position (z).

TABLE I. Coefficients of the three regions of the third-order cross-correlator measurement.

Region of laser temporal footprint	Peak	Shoulder	Pedestal
Normalized amplitude (A)	1	3.27×10^{-4}	5.4×10^{-8}
Temporal offset (μ) (ps)	0	3.0×10^{-1}	5.57×10^{-1}
Gaussian width (σ) (ps)	0.017[a]	1.1	6.47

[a]17 fs corresponds to a 40 fs FWHM (FWHM $= 2\sigma\sqrt{2\ln 2}$) pulse duration measured by a GRENOUILLE.

TABLE II. Fit parameters to each of the material surfaces studied during plasma mirror characterization.

PM surface	Pol.	Ionization intensity (W/cm^2)	Expansion velocity c_s(cm/s)	Absorption (%)
VHS plastic surface	S	6.4×10^{13}	1.8×10^7	18
VHS plastic surface	P	6.4×10^{13}	1.8×10^7	48
VHS iron oxide surface	S	1.6×10^{13}	1.5×10^7	19
VHS iron oxide surface	P	1.6×10^{13}	1.5×10^7	46

The first fit parameter is the ionization intensity (I_{Ionize}) needed to produce the surface plasma. The fitting values we used, given in Table II, match in agreement with previous publications of femtosecond-class laser ionization of solids.[15–17] Following ionization, the collisional ionization increases plasma density above critical density in the creation of a PM.[7]

The ionization intensity was used to fit the width of the drop in reflectance, shown in Fig. 4, when focusing near z = 0 mm. Changing the ionization level has a dramatic effect on the width of the drop in reflectance around z = 0 mm (as shown in Fig. 7(c)). This was seen when changing which surface of the VHS tape was used to create the PM in Fig. 4. Mylar has a higher ionization threshold than iron, which is seen in the ideal fitting parameters, and mylar produces a much narrower drop in reflectance. Iron's lower ionization threshold can be reached on the tape surface further from focus, producing a wider dip in reflectance around z = 0 mm.

As the focus of the laser was further from the tape, the intensity far off-axis eventually drops below the ionization threshold before the peak arrives. This results in a gradual drop in reflectance seen when focusing far from the tape and is explained in Section IV C as the Spatial Reflectance term, S(z).

The second fit parameters are the expansion velocity (c_s) of the plasma ions. The expansion velocity of the plasma is given by the ion sound speed, $c_s = \sqrt{Zk_BT_e/m_i}$, with Z as the charge of the ion, k_B is Boltzmann's constant, T_e is the electron temperature, and m_i is the mass of the ion. Because it is not easy to determine the exact charge state of an ion during a complex ionization, we used the expansion velocity as a fitting parameter, and its use is heuristic in order to gain insights into the complexity of the self-triggering PM. Similar to how the ionization level determined the width of the drop in reflectance around z = 0 mm, choosing the correct expansion velocity will optimally fit the depth of the drop in reflectance around z = 0 mm [as shown in Fig. 7(b)]. A larger expansion velocity will have a sharper drop in reflection and a deeper drop (between maximum and minimum reflectance values) in the reflectance curves around the point of minimum reflectance. This can also be seen in Fig. 4 when comparing the fitting curves for VHS iron oxide surface and VHS plastic surface to their respective counterpart of the same polarization. The expansion velocity for the VHS plastic surface is greater than that of the VHS iron oxide surface, which results in the greater change between the maxima and minima of the reflectance curves, and a sharper drop off between the two maxima. We used the ion sound velocities which are in agreement with previous PM publications.[7,17–19]

The final fit parameter is the absorption percentage (α) of the input light. The absorption levels of 18%–19% seen in the study of s-polarized light agree with previously published values from a self-triggered PM.[7,19,20] The absorbed energy directly relates to a drop in reflectance (as shown in Fig. 7(d)), and this parameter is used to vertically shift the plot to match the height of the experimental data. The difference between the absorption values for scans of s-polarized and p-polarized input light were the result of Brunel[12] and resonance absorption.[13]

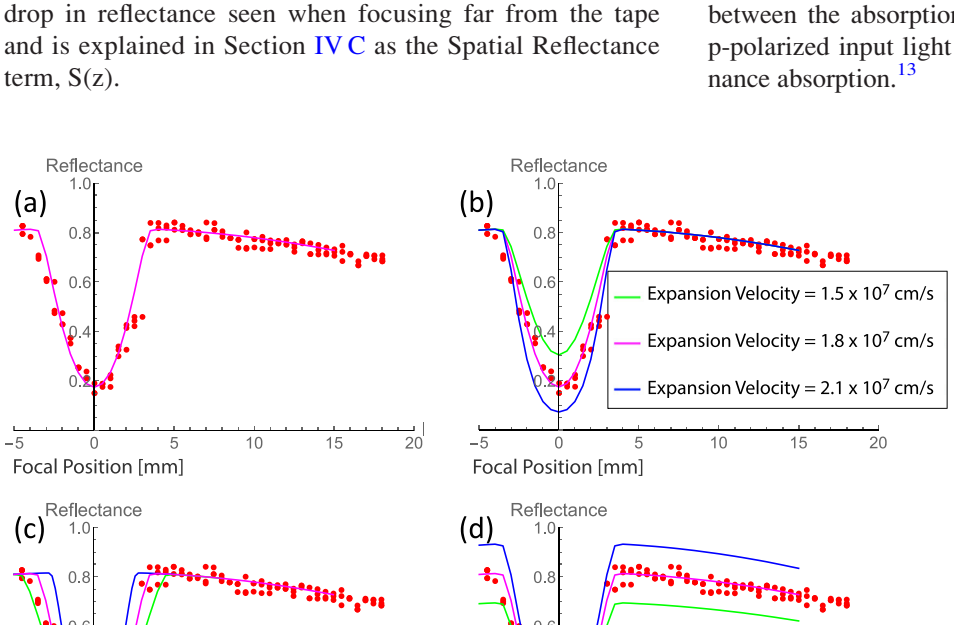

FIG. 7. (a) The best fit to the case of s-polarized light incident on the VHS plastic surface using the best fitting parameters, which are given in the first row of Table II. The effects of changing the expansion velocity [subplot (b)], the ionization intensity [subplot (c)], and the amount of absorbed energy [subplot (d)] are shown for each fitting parameter independently. The focal position for each plot is measured relative to the tape surface.

The values for each fit parameter used to best fit our experimental data are given in Table II.

Figure 7 shows how changing each plasma parameter would affect the curve's fits to the experimental data. Figure 7(b) shows the affect of changing the expansion velocity of the model by $\pm 3 \times 10^6$ cm/s. Changing the expansion velocity has a noticeable effect on the minimum value of reflectance at z = 0 mm. Figure 7(c) shows the affect of changing the ionization intensity within the model by $\pm 3.2 \times 10^{13}$ W/cm^2. Varying the ionization intensity has a noticeable change in the width in the drop of reflectance around z = 0 mm. Figure 7(d) illustrates the affect of altering the amount of absorbed energy by the PM within the model by ±12%. Adjusting the amount of absorbed energy scales the entire reflectance curve vertically, because higher absorption directly correlates to a lower reflectance.

The fact that the variation of each of the discussed parameters changes a different characteristic of the reflectance curve allows an independent measurement of the individual plasma parameters.

C. Spatial reflectance term

Assuming a Gaussian distribution of intensity, regions further from the center of the spot contain less energy than regions near the center. A spatial reflectance term, S(z), calculates the percentage of the laser's spot energy above the ionization threshold to trigger the plasma mirror prior to the peak of the pulse. This term produces the gradual drop in reflectance when focusing far from the tape.

To calculate the maximum radius at which ionization occurs, we solve for R_{Ionize} in the equation

$$I_{Tape} e^{-2R_{Ionize}^2/w(z)^2} = I_{Ionize}. \tag{5}$$

Then we calculate the fraction of the laser's spot size which had an intensity above the ionization level, by taking the integral

$$S(z) = \frac{\int_0^{R_{Ionize}} \left(I_{Tape} e^{-2r^2/w(z)^2}\right) r\, dr}{\int_0^{\infty} \left(I_{Tape} e^{-2r^2/w(z)^2}\right) r\, dr}. \tag{6}$$

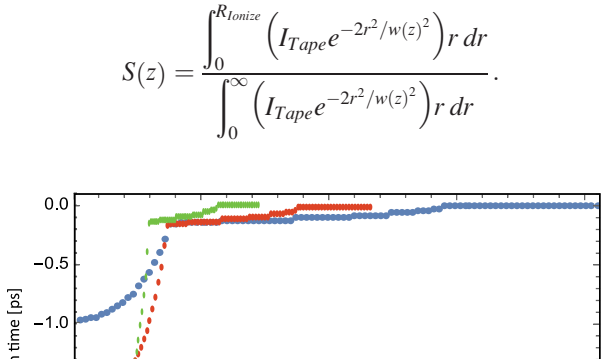

FIG. 8. Plot showing the ionization time at each radius r within the spot size on the tape using s-polarized light from the VHS plastic surface. The ionization intensity in this case was 6.4×10^{13} W/cm^2.

Here, the numerator solves for only the ionized portion of the spot, and the denominator calculates the entire intensity within the full spot.

D. Reflectance algorithm

The equation used to model the reflectance from the PM assumes a statistical treatment of an electromagnetic waves incident on a normally distributed surface is given in Refs. 20 and 21. The amount of light reflected from the PM was calculated from

$$r(z) = I_R/I_0 = \exp\left[-\left(\frac{4\pi\sigma_r}{\lambda}\cos\theta_i\right)^2\right], \tag{7}$$

at each focal position z. In order to find the roughness σ_r of the PM surface, the algorithm is:

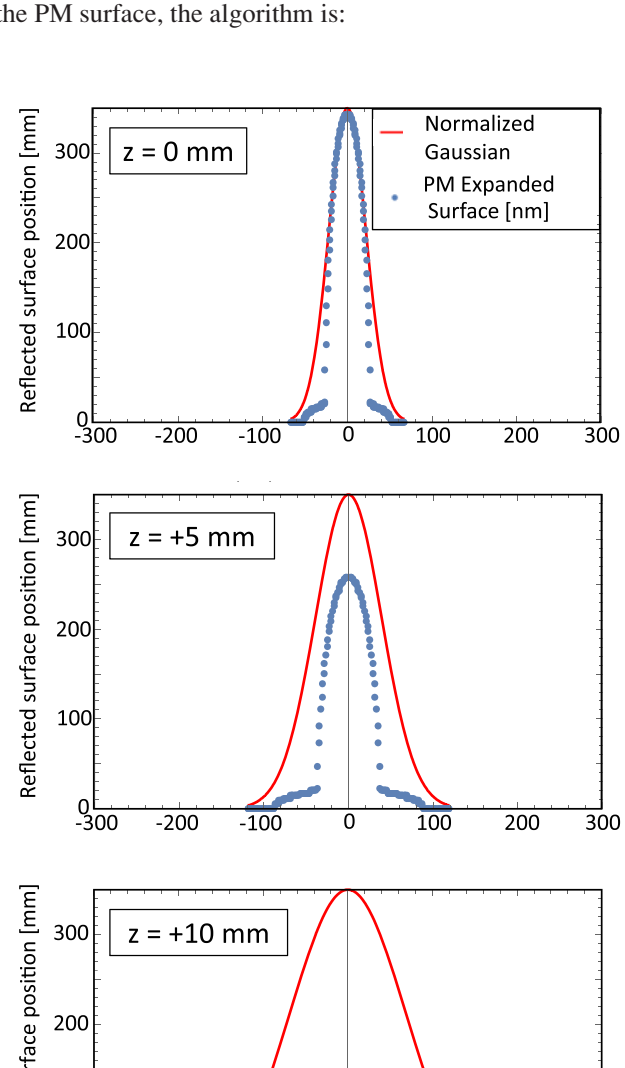

FIG. 9. Plots showing the shape of the PM reflective surface for a focal scan using s-polarized light from the VHS plastic surface. The expansion velocity in this case was 1.8×10^7 cm/s (or equivalently 180 nm/ps).

- The time at which ionization occurs (t_0) must be calculated at each radial position (r) within the spot size on the tape. This was done by assuming a Gaussian spot on the tape of the form $e^{-2r^2/w(z)^2}$ and the temporal intensity profile I(t) given in Eqs. (2)–(3). The ionization time was calculated by solving for the time which the function $I(z,t)e^{-2r^2/w(z)^2} = I_{Ionize}$. This gives an array for the ionization time t_0 at each radial position r. The results of this step are shown in Fig. 8.
- By multiplying the ionization time by the expansion velocity c_s, the position of the PM surface when the peak of the laser pulse arrives (at time t = 0) was solved for at each radial location. The plasma expansion is assumed to be adiabatic and the PM surface at which reflection occurs. For a laser pulse incident on a plasma with an exponential density gradient, reflection occurs at a density $n = n_{crit}\cos^2(\theta)$, where $\theta = 45^\circ$ in this case and $n_{crit} = 1.7 \times 10^{21}\,\mathrm{cm}^{-3}$. While plasma heating would imply an increasing velocity following ionization, a constant value of c_s is used as the average velocity of the PM surface between ionization and reflection times. The results of this step are shown in Fig. 9.
- The standard deviation of the surface positions was interpreted as σ_r. The range over which σ_r is calculated includes the radii within the spot which become ionized prior to the main peak of the laser pulse.
- This process was repeated for each value of z within the focal scan; resulting in a value of σ_r at each z-location.
- Once the plasma surface roughness $\sigma_r(z)$ was found for the ionized PM at each focal location, we recall Eq. (7) to find $I_R(z)$.

E. Model fit parameter results

The results for each of the fitting parameters used to fit the PM experimental data are given in Table II. The resulting plots for each of the reflectance model using the fit parameters from Table II are shown in Fig. 10 for the VHS tape polarization study.

For different peak intensities, the plasma will ionize at different times before the main pulse. The higher ionization intensity for the VHS plastic surface was responsible for the narrow dip in reflectance when the focus was positioned on or near the tape surface. The VHS iron oxide surface has a lower ionization intensity, which allows for the solid to be ionized when the focus was positioned further from tape surface.

The higher ionization intensity of the VHS plastic surface of $6.4 \times 10^{13}\,\mathrm{W/cm^2}$ also produces a higher electron expansion velocity of 1.8×10^7 cm/s. Since the surface was ionized at a higher intensity than the VHS iron oxide surface, the electrons have less time to expand, because they become ionized later in time and closer to the peak of the laser pulse. This results in the electrons expanding a shorter distance in case of the VHS plastic surface, and a minimum reflectance of $18\% - 20\%$ was seen when the focus was positioned at the surface of the VHS plastic surface. The VHS iron oxide has more time to expand, with an electron expansion velocity of 1.5×10^7 cm/s, following ionization at an intensity of $1.6 \times 10^{13}\,\mathrm{W/cm^2}$. This resulted in a minimum reflectance of $5\% - 10\%$ when the focus was positioned on the VHS iron oxide surface.

The absorbed energy values were used to fit the vertical range of the experimental data. Our maximum reflectance of 82% was a result of the picosecond contrast of the laser and the high ionization intensity needed to ionize the VHS plastic surface. This reflectance matches the values previously published with similar contrasts and intensities for s-polarized pulses reflecting from a PM.[7,19,20]

Changing the input light's polarization from s-polarized to p-polarized provided a direct comparison of the magnitude

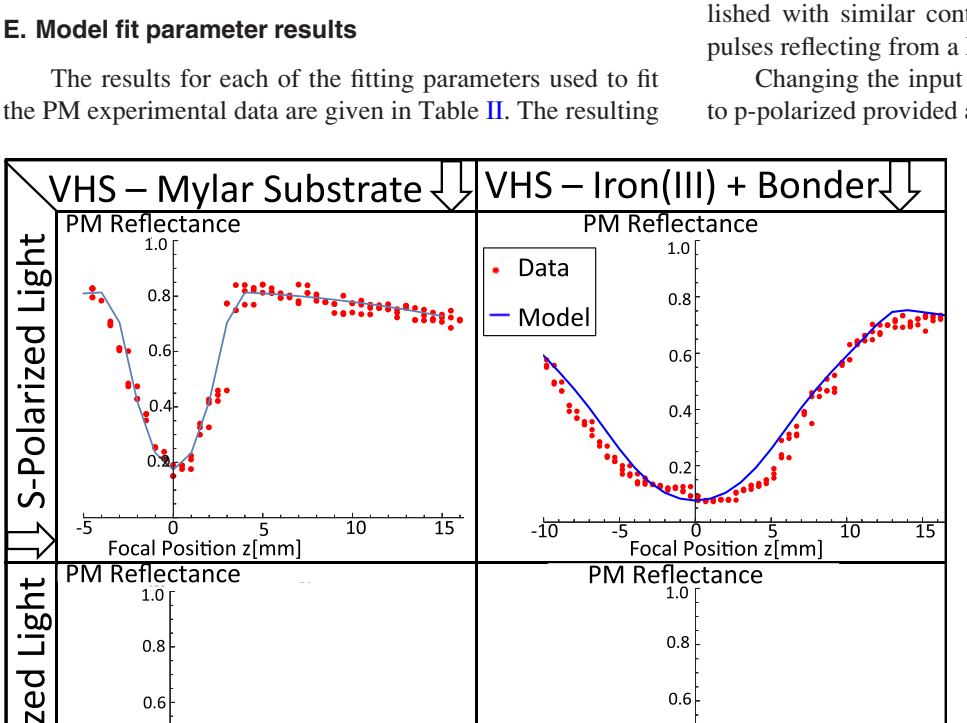

FIG. 10. Plots showing the match between the PM model and the experimental data of both VHS plastic and iron oxide surfaces, using S and P-polarized light.

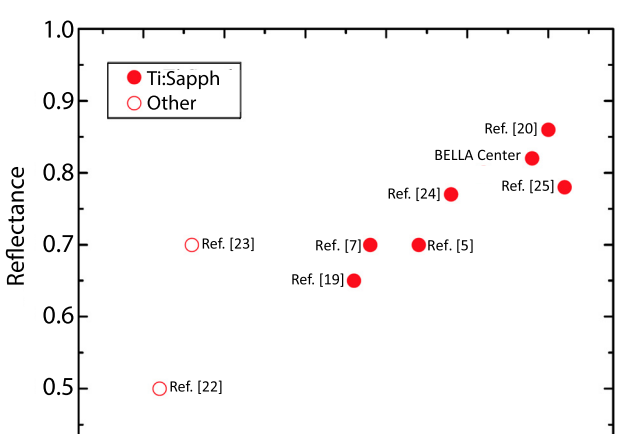

FIG. 11. Plasma Mirror reflectances of s-polarized lasers at 45° plotted against publication year. The publications in the figure refer to: 1991 Ref. 22, 1993 Ref. 23, 2003 Ref. 19, 2004 Ref. 7, 2007 Ref. 5, 2009 Ref. 24, 2014 refers to data from this paper, 2015 Ref. 20, and 2016 Ref. 25.

of the total absorption processes for each polarization of light interacting with an expanding plasma surface. Changing the polarization increased the absorption values from 18% to 48% from the VHS plastic surface and 19% to 46% from the VHS iron oxide surface. This increase in absorption of 27%–30% corresponds to a direct measurement of the contributions of resonance and Brunel absorption.

A plot showing the published reflectance values from different PM studies and the year they were measured is given in Fig. 11. There is a clear trend that the published values of reflectance have increased continually over the past 10–15 years as a result of an increased temporal intensity contrast of the laser systems itself. Saturable absorbers[26] are capable of suppressing pre-pulses on a ns time scale by 1–2 orders of magnitude. Double-Chirped Pulse Amplification (double-CPA) systems[27] applying nonlinear filters, such as cross-polarized wave generation (XPW),[28] achieve a pre-pulse suppression by up to 3 orders of magnitude. The concept of Optical Parametrical CPA (OPCPA)[29] mitigates prepulse generation by using pump laser with short pulses (fs-ps).

The maximum reflectance seen from a PM is 96% which was published by Scott *et al.* in Ref. 20. This record PM reflectance was produced by pre-ionizing the PM surface using a controlled prepulse before the peak of the laser arrived.

V. SUMMARY

A tape drive has been developed to provide a fresh (undamaged) surface as PM for successive, focused high intensity laser pulses. This helps overcome the challenge that is created for PM experiments, which is that the laser produced surface plasma is destructive to the optic, significantly reducing the lifetime of an optic.

A pointing study showed that the pointing fluctuations caused by the PM were $\simeq 1$ mrad ($\theta_{PM} = 0.94$ mrad in x and $\theta_{PM} = 1.0$ mrad in y). Nearly a third of this pointing fluctuation ($\theta_{Tape} = 310\ \mu$rad) is attributed to the spooling mechanics of the tape drive.

The reflectance polarization study of the PM gave a direct comparison of s and p-polarized light reflected from the iron oxide and plastic surface of the VHS tape. These experimental data also showed a peak in reflectance from the VHS plastic surface at ± 4 mm from the tape surface. The wavefront was also confirmed to be conserved. This makes the tape based plasma mirror a novel optic for experiments which require high quality beams to be pointed near their final focal plane.

The theoretical plasma mirror model provided a match between the experimental data and a statistical treatment of electromagnetic waves incident on a normally distributed surface roughness. Varying the laser intensity on the tape surface by changing the laser focal position and measurement of the PM reflectance allowed for the first time, the determination of the plasma parameters, I_{Ionize}, c_s, and α in one experimental scan in good agreement with previously published methods. This provided insight into details of the PM expansion dynamics and a direct measurement of the combined contribution of absorption mechanisms for each polarization of light.

ACKNOWLEDGMENTS

This work was supported by the U.S. Department of Energy Office of Science Office of High Energy Physics, under Contract No. DE-AC02-05CH11231, by the U.S. Department of Energy National Nuclear Security Administration, Defense Nuclear Nonproliferation R&D (NA22), and by the National Science Foundation (NSF) under Contract Nos. 0917687 and 0935197.

[1]B. H. Shaw, J. van Tilborg, T. Sokollik, C. B. Schroeder, W. R. McKinney, N. A. Artemiev, V. V. Yashchuk, E. M. Gullikson, and W. P. Leemans, J. Appl. Phys. **114**, 043106 (2013).
[2]J. van Tilborg, B. Shaw, T. Sokollik, S. Rykovanov, S. Monchocé, F. Quéré, P. Martin, A. Malvache, and W. Leemans, Opt. Lett. **38**, 4026 (2013).
[3]I. Kim, I. Choi, S. Lee, K. Janulewicz, J. Sung, T. Yu, H. Kim, H. Yun, T. Jeong, and J. Lee, Appl. Phys. B **104**, 81 (2011).
[4]C. Rödel, M. Heyer, M. Behmke, M. Kübel, O. Jäckel, W. Ziegler, D. Ehrt, M. Kaluza, and G. Paulus, Appl. Phys. B **103**, 295 (2011).
[5]A. Lévy, T. Ceccotti, P. D'Oliveira, F. Réau, M. Perdrix, F. Quéré, P. Monot, M. Bougeard, H. Lagadec, P. Martin *et al.*, Opt. Lett. **32**, 310 (2007).
[6]T. Wittmann, J.-P. Geindre, P. Audebert, R. Marjoribanks, J.-P. Rousseau, F. Burgy, D. Douillet, T. Lefrou, K. T. Phuoc, and J.-P. Chambaret, Rev. Sci. Instrum. **77**, 083109 (2006).
[7]G. Doumy, F. Quéré, O. Gobert, M. Perdrix, P. Martin, P. Audebert, J. Gauthier, J.-P. Geindre, and T. Wittmann, Phys. Rev. E **69**, 026402 (2004).
[8]E. D. Daniel, C. D. Mee, and M. H. Clark, *Magnetic Recording: The First 100 Years* (Wiley, 1999).
[9]J. van Tilborg, S. Steinke, C. Geddes, N. Matlis, B. Shaw, A. Gonsalves, J. Huijts, K. Nakamura, J. Daniels, C. Schroeder *et al.*, Phys. Rev. Lett. **115**, 184802 (2015).
[10]S. Steinke, J. van Tilborg, C. Benedetti, C. Geddes, C. Schroeder, J. Daniels, K. Swanson, A. Gonsalves, K. Nakamura, N. Matlis *et al.*, Nature **530**, 190 (2016).
[11]S. Shiraishi, *Investigation of Staged Laser-Plasma Acceleration* (Springer, 2014).
[12]F. Brunel, Phys. Rev. Lett. **59**, 52 (1987).
[13]J. Freidberg, R. Mitchell, R. L. Morse, and L. Rudsinski, Phys. Rev. Lett. **28**, 795 (1972).
[14]R. Trebino, *Frequency-Resolved Optical Gating: The Measurement of Ultrashort Laser Pulses* (Springer Science & Business Media, 2012).

[15]X. Wang and M. Downer, Opt. Lett. **17**, 1450 (1992).
[16]B.-T. V. Vu, O. L. Landen, and A. Szoke, Phys. Rev. E **47**, 2768 (1993).
[17]B.-T. Vu, A. Szoke, and O. Landen, Phys. Rev. Lett. **72**, 3823 (1994).
[18]B. Dromey, S. Kar, M. Zepf, and P. Foster, Rev. Sci. Instrum. **75**, 645 (2004).
[19]C. Ziener, P. Foster, E. Divall, C. Hooker, M. Hutchinson, A. Langley, and D. Neely, J. Appl. Phys. **93**, 768 (2003).
[20]G. Scott, V. Bagnoud, C. Brabetz, R. Clarke, J. Green, R. Heathcote, H. Powell, B. Zielbauer, T. Arber, P. McKenna *et al.*, New J. Phys. **17**, 033027 (2015).
[21]A. Spizzichino and P. Beckmann, *The Scattering of Electromagnetic Waves from Rough Surfaces* (Pergamon, New York/Paris, 1963).
[22]H. C. Kapteyn, A. Szoke, R. W. Falcone, and M. M. Murnane, Opt. Lett. **16**, 490 (1991).
[23]S. Backus, D. M. Gold, H. Nathel, H. C. Kapteyn, M. M. Murnane, and W. White, Opt. Lett. **18**, 134 (1993).
[24]A. Henig, S. Steinke, M. Schnürer, T. Sokollik, R. Hörlein, D. Kiefer, D. Jung, J. Schreiber, B. Hegelich, X. Yan *et al.*, Phys. Rev. Lett. **103**, 245003 (2009).
[25]D. Schumacher, private communications (2016).
[26]J. Itatani, J. Faure, M. Nantel, G. Mourou, and S. Watanabe, Opt. Commun. **148**, 70 (1998).
[27]M. Kalashnikov, E. Risse, H. Schönnagel, A. Husakou, J. Herrmann, and W. Sandner, Opt. Express **12**, 5088 (2004).
[28]A. Jullien, O. Albert, F. Burgy, G. Hamoniaux, J.-P. Rousseau, J.-P. Chambaret, F. Augé-Rochereau, G. Chériaux, J. Etchepare, N. Minkovski *et al.*, Opt. Lett. **30**, 920 (2005).
[29]A. Dubietis, G. Jonušauskas, and A. Piskarskas, Opt. Commun. **88**, 437 (1992).